Cell Metabolism
Article

Lymphatic Vessels Are Essential for the Removal of Cholesterol from Peripheral Tissues by SR-BI-Mediated Transport of HDL

Hwee Ying Lim,[1] Chung Hwee Thiam,[1] Kim Pin Yeo,[1] Radjesh Bisoendial,[2] Chung Shii Hii,[1] Kristine C.Y. McGrath,[3] Kar Wai Tan,[1,4] Alison Heather,[3] J. Steven Jonathan Alexander,[5] and Veronique Angeli[1,*]
[1]Department of Microbiology, Immunology Programme, Yong Loo Lin School of Medicine, National University of Singapore, Singapore 117597, Republic of Singapore
[2]Heart Research Institute and Centenary Institute Newtown, Sydney, NSW 2042, Australia
[3]School of Medical and Molecular Biosciences, Faculty of Science, University of Technology, Sydney, NSW 2007, Australia
[4]Singapore Immunology Network, BMSI, A-STAR, Singapore 138648, Republic of Singapore
[5]Department of Molecular and Cellular Physiology, LSU Health Sciences Center, Shreveport, LA 71130, USA
*Correspondence: micva@nus.edu.sg
http://dx.doi.org/10.1016/j.cmet.2013.04.002

SUMMARY

Removal of cholesterol from peripheral tissues to the bloodstream via reverse cholesterol transport (RCT) is a process of major biological importance. Here we demonstrate that lymphatic drainage is required for RCT. We have previously shown that hypercholesterolemia in mice is associated with impaired lymphatic drainage and increased lipid accumulation in peripheral tissues. We now show that restoration of lymphatic drainage in these mice significantly improves cholesterol clearance. Conversely, obstruction of lymphatic vessels in wild-type mice significantly impairs RCT. Finally, we demonstrate using silencing RNA interference, neutralizing antibody, and transgenic mice that removal of cholesterol by lymphatic vessels is dependent on the uptake and transcytosis of HDL by scavenger receptor class B type I expressed on lymphatic endothelium. Collectively, this study challenges the current view that lymphatic endothelium is a passive exchange barrier for cholesterol transport and provides further evidence for its interplay with lipid biology in health and disease.

INTRODUCTION

Reverse cholesterol transport (RCT) is a multistep process whereby excess cholesterol is transported by high-density lipoprotein (HDL) from the peripheral tissues to the liver for excretion in the bile and feces (Rader et al., 2009; Tall, 2008). The initial and final steps in RCT, including cholesterol efflux from macrophages to extracellular HDL and cholesterol uptake in the liver for disposal as biliary cholesterol and bile salts, respectively, have been extensively studied and well characterized. In contrast, much less information is available on the route by which HDL cholesterol travels from the peripheral tissues to the liver.

Since one of the major roles of the lymphatic system is to drain macromolecules from the interstitial space back to the circulation, it is generally assumed that the return of lipoproteins from the interstitium to plasma may occur primarily via the lymphatic system, and less so via the venous capillaries (Cooke et al., 2004). Although several lines of evidence support this scenario, it has not been directly demonstrated. Analyses of the composition of animal and human lymph revealed that lymph is rich in cholesterol and HDL (Nanjee et al., 2001; Reichl, 1990; Roheim et al., 1990) and the composition in lipoproteins varies with changes in lymphatic flow (Cooke et al., 2004). In a more detailed study of the different lipoproteins fractions in human lymph, it was shown that the lymph concentration of HDL cholesterol was 30% greater than that of blood, and the authors estimated a whole-body reverse cholesterol transport rate of 344 mg/day via the lymph (Nanjee et al., 2001). However, the lymph/plasma concentration ratios of lipoprotein reported by Nanjee et al. should be considered with care, as they contradict data by other groups (Sloop et al., 1987). Analysis of the transport of labeled cholesterol after intravenous injection in humans indicated that some of the cholesterol detected in lymph was derived from a pool of tissue cholesterol (Reichl et al., 1973).

Clinical and experimental studies have linked lymphatic function to lipid metabolism and transport (Dixon, 2010). Obstructions of lymphatic vessels in mouse not only account for architectural tissue changes, edema, and infiltration of immune cells, but also abnormal lipid accumulation in the skin (Rutkowski et al., 2006). In addition, massive lipid deposits are also evident in the edematous tissues of patients with lymphedema (Schirger et al., 1962). Recently, we demonstrated that hypercholesterolemic apolipoprotein E-deficient (apoE$^{-/-}$) mice develop lymphatic dysfunction and exhibit peripheral edema (Lim et al., 2009). This edema was associated with marked lipid accumulation. These observations led us to propose that hypercholesterolemia may impair lymphatic function, and this loss of function could further exacerbate the accumulation of cholesterol and worsen edema in the peripheral tissues. However, the question as to whether restoration of lymphatic function in apoE$^{-/-}$ mice would ameliorate the accumulation of lipids and edema remained to be addressed.

Despite the recent advances in understanding lymphatic vessel structure and function, our current knowledge of the basic mechanisms involved in lymphatic lipid transport is relatively poor. The entry of fluid, macromolecules, and cells mainly occurs throughout initial lymphatic vessels, which are blind-ended vessels lacking smooth muscle cells via openings between button-like junctions (Baluk et al., 2007). The initial lymphatic vessels converge into larger collecting vessels that exhibit smooth muscle cells on their outer wall to actively pump the lymph back to the blood circulation (Muthuchamy and Zawieja, 2008). Maintenance of initial and collecting vessel structure is critical for lymphatic function (Lim et al., 2009; Petrova et al., 2004). Although the prevailing view is that lymphatic vasculature plays a passive role in the uptake of fluid, macromolecules, and cells, increasing evidence suggests a more active role of lymphatic vessels than previously anticipated. Recent studies on the mechanisms of leukocyte entry through lymphatics revealed the involvement of specialized entry sites (Baluk et al., 2007; Pflicke and Sixt, 2009) and molecules expressed on the lymphatic endothelium including adhesion molecules and chemokines (Johnson and Jackson, 2010; Schumann et al., 2010; Tal et al., 2011). Thus, these findings raise the possibility that the removal of cholesterol by lymphatic vessels may also be a specific and active process, and, if confirmed, this would imply that the lymphatic endothelium may be able to control the composition of lipoprotein in tissue fluid and lymph.

In light of the emerging significance of lymphatic vessel in lipid metabolism and transport in health and disease, we decided to evaluate the contribution of lymphatic vessels in the clearance of lipoproteins from peripheral tissues and to identify the mediators involved in this process.

RESULTS

Reversing Dyslipidemia in apoE$^{-/-}$ Mice Restores the Structure and Function of Lymphatic Vessels

We hypothesized that reduction of circulating cholesterol levels and increase of HDL levels in apoE$^{-/-}$ mice may restore lymphatic structure and function. To address this, we measured the effect of the reduction of plasma cholesterol levels in apoE$^{-/-}$ mice by using the cholesterol-lowering drug ezetimibe, which blocks dietary and biliary cholesterol absorption from the intestine. Consistent with other reports (Davis et al., 2001; Kuhlencordt et al., 2009), total plasma cholesterol levels in apoE$^{-/-}$ mice fed a high-fat diet were significantly reduced by 4 weeks of ezetimibe treatment and maintained below 600 mg/dl throughout the whole duration of treatment regime (Figures S1A–S1C available online). In contrast, vehicle-treated apoE$^{-/-}$ mice had grossly elevated cholesterol levels (>2,000 mg/dl), as we reported previously (Lim et al., 2009) (Figure S1A). Treatment with ezetimibe also markedly increased plasma HDL cholesterol in apoE$^{-/-}$ mice to levels similar to those in wild-type (WT) mice (Figure S1B). Ezetimibe did not have any effect on total cholesterol or HDL cholesterol in WT mice (Figures S1A and S1B). In the following experiments, vehicle-treated WT mice were used as control for comparison with vehicle-treated apoE$^{-/-}$ mice.

In agreement with our previous study (Lim et al., 2009), microscopic analysis of ear skin whole mount with lymphatic vessel endothelial hyaluronan receptor 1 (LYVE-1) showed hyperplasic initial lymphatic vessels in vehicle-treated apoE$^{-/-}$ mice (Figure 1A). With ezetimibe treatment, initial lymphatic vessels were substantially less dilated (Figure 1B). Consistent with previous reports (Petrova et al., 2004; Lim et al., 2009), collecting vessels in WT mice downregulated LYVE-1 and were endowed with smooth muscle cells, whereas LYVE-1 remained highly expressed and smooth muscle cell coverage was sparse on collecting lymphatic vessels from vehicle-treated apoE$^{-/-}$ mice (Figure 1C). However, amelioration of dyslipidemia in these mice restored the identity of collecting vessels (Figure 1C). We next investigated the functionality of these vessels. Evans blue dye lymphangiography is a standard method for assessing lymphatic function (Danussi et al., 2008). After intradermal injection of Evans blue dye into the ear rim, fine distinct lymphatic vessels were visualized in ezetimibe-treated apoE$^{-/-}$ mice as observed in WT mice, demonstrating that these lymphatic vessels are functional (Figure 1D). In contrast, vehicle-treated apoE$^{-/-}$ mice showed markedly dilated lymphatic vessels, and Evans blue dye extravasated from these dilated vessels (Figure 1D). As an alternative measure of lymphatic function, we analyzed the capacity of lymphatic vessels to transport dendritic cells from the peripheral tissue to the draining lymph nodes (LNs). Consistent with our previous report (Angeli et al., 2004), the migration of skin dendritic cells in apoE$^{-/-}$ was significantly impaired compared to WT mice (Figure 1E), but it was improved by ezetimibe treatment (Figure 1E).

Amelioration of Lymphatic Drainage in apoE$^{-/-}$ Mice Reduces Cholesterol Accumulation in Tissues

We next determined whether this improved lymphatic drainage in ezetimibe treated apoE$^{-/-}$ mice had some consequences on the peripheral edema and lipid accumulation observed in apoE$^{-/-}$ mice (Lim et al., 2009; van Ree et al., 1995). Macroscopic examination of the footpad revealed exaggerated swelling in vehicle-treated apoE$^{-/-}$ mice compared to WT mice (1.942 ± 0.028 mm versus 1.603 ± 0.019 mm, n = 11–16, $p < 0.0001$), and ezetimibe treatment ameliorated this swelling (1.630 ± 0.021 mm, n = 11–16, $p < 0.0001$) (Figure 2A). Furthermore, oil red O staining and measure of total cholesterol in footpads demonstrated that this attenuated swelling in ezetimibe-treated apoE$^{-/-}$ mice was, in part, associated with a decrease in the neutral lipid and cholesterol deposition in these tissues (Figures 2B and 2C). As also reported in several animal models of hypercholesterolemia (Armstrong et al., 1986; Ishibashi et al., 1994; van Ree et al., 1995), the skin of apoE$^{-/-}$ mice exhibited accumulation of macrophages and xanthomas, which consist of cholesterol-rich deposits, particularly rich in macrophages (Figures 2B–2D). Notably, total macrophages (Figure 2D) and lipid-laden macrophages (Figure 2E) were less abundant in ezetimibe-treated apoE$^{-/-}$ mice with improved lymphatic drainage. Altogether, these findings suggest that reduction of plasma total cholesterol and increase of HDL in apoE$^{-/-}$ mice restored lymphatic function and, hence, lipid, fluid, and leukocyte clearance from peripheral tissues. Similar results were obtained in another murine model of hypercholesterolemia and atherosclerosis, the Ldlr$^{-/-}$ mice, further supporting the physiological relevance of our observations (Figure S2).

In an effort to identify the mediators responsible for the defects in lymphatic vessels from apoE$^{-/-}$ mice, we performed

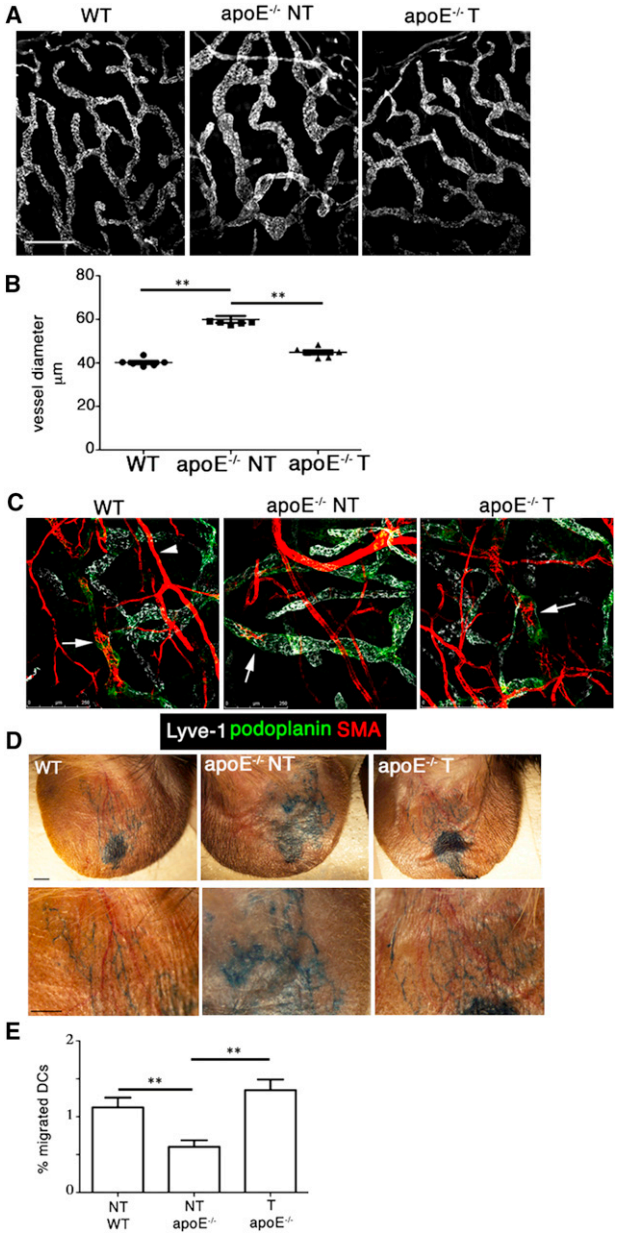

Figure 1. Restoration of Lymphatic Vessel Structure and Function in apoE$^{-/-}$ Mice by Reducing Hypercholesterolemia

(A–C) LYVE-1 immunostaining was examined in ear whole mounts from WT and apoE$^{-/-}$ mice after 12 weeks of treatment with vehicle (NT) or ezetimibe (T) (A). The diameter of initial lymphatic vessels was quantified with n = 6 and **p < 0.005 (B). Ear whole mounts were stained with LYVE-1, smooth muscle actin (SMA), and podoplanin for identification of collecting lymphatic vessels (C). Arrows indicate smooth muscle cells. Smooth muscle actin also stained for blood vessels (arrowheads). Images are representative of two repeated experiments, and n = 4 per group (A and C). Scale bars represent 400 μm in (A) and 250 μm in (C).

(D and E) Evans blue lympahgiography was performed (D). Similar results were obtained in three repeated experiments. Scale bars represent 1.0 mm. For quantification of DC migration to draining LNs, mice received epicutaneous FITC and the percentage of migrated FITC$^+$CD11c$^+$ DCs in draining LNs was determined (E). Data are pooled from two independent experiments with n = 7–13.

**p < 0.005. Data are shown as mean ± SEM. See also Figure S1.

quantitative real-time PCR analyses on skin from vehicle-treated WT and apoE$^{-/-}$ mice and ezetimibe-treated apoE$^{-/-}$ mice. This analysis revealed that the expression of VEGF-C, ANG-2, and FOXC2 (Tammela and Alitalo, 2010), which are important factors to maintain lymphatic vasculature, was significantly reduced in apoE$^{-/-}$ vehicle-treated mice (Figure 3A). No differences were observed for VEGF-A, VEGF-D and bFGF. Lowering cholesterol in apoE$^{-/-}$ mice with ezetimibe significantly increased VEGF-C, ANG-2, and FOXC2 expression to levels similar to WT mice (Figure 3A). Because treatment with VEGF-C has been shown in other models to improve lymphatic drainage (Szuba et al., 2002; Breslin et al., 2007), we investigated whether local injection of VEGF-C could ameliorate lymphatic function and cholesterol accumulation in apoE$^{-/-}$ mice. To evaluate lymphatic function in a more quantitative manner than Evans blue lymphangiography, we measured the transport of fluorescein isothiocyanate (FITC) dextran from the footpad to the draining LN. This assay confirmed the dysfunctional lymphatic vessels in apoE$^{-/-}$ mice (Figure 3B) and demonstrated that VEGF-C treatment significantly improved lymphatic function in apoE$^{-/-}$ mice (Figure 3C). Furthermore, amelioration of lymphatic function in apoE$^{-/-}$ mice significantly reduced the accumulation of cholesterol in the footpads, and this effect did not result from reduced hypercholesterolemia (Figures 3D and 3E). These data showed that improvement of lymphatic function without affecting hypercholesterolemia can be sufficient to reduce cholesterol accumulation in apoE$^{-/-}$ mice.

Lymphatic Drainage Is Required for Cholesterol HDL Transport from Peripheral Tissue into Blood Circulation

The close relationship between lymphatic drainage dysfunction and lipid accumulation in peripheral tissue observed in apoE$^{-/-}$ mice raised the possibility that, under physiological conditions, RCT may depend on lymphatic vessels and that adequate lymphatic transport may be necessary to limit excessive accumulation of cholesterol in tissues. To address this possibility, we tested whether impaired lymphatic drainage would affect RCT. We adapted and recapitulated a RCT model using fluorescence-labeled cholesterol instead of radiolabeled cholesterol. First, we confirmed in vitro that this fluorescent cholesterol was efficiently effluxed from macrophages in presence of HDL and that this fluorescent-cholesterol efflux was also mediated by ATP-binding cassette transporter A1 (ABCA1) using probucol (Figures S3A and S3B). We also confirmed in vivo that the fluorescent cholesterol was transported into the plasma and feces after intraperitoneal injection of macrophages loaded with the fluorescent cholesterol as described in original studies using radiolabeled cholesterol (Figure S3C) (Wang et al., 2007; Zhang et al., 2003). Next, we evaluated in vivo the levels of fluorescence after the deposition of fluorescent-cholesterol-loaded macrophages in the footpad. Consistent with previous studies using radiolabeled cholesterol, we were able to detect fluorescent cholesterol in plasma, liver, and feces of WT mice (Figure 4). A significant amount of fluorescent cholesterol was removed from the site of injection by 48 hr (Figure 4A) and was found within the LN draining the site of injection and in the efferent lymph as soon as 6 hr (Figures 4B and 4C). Fluorescent cholesterol was only detected in plasma by 12 hr (Figure 4D), 48 hr, and 72 hr in liver and feces, respectively (Figures 4E and 4F). The plasma

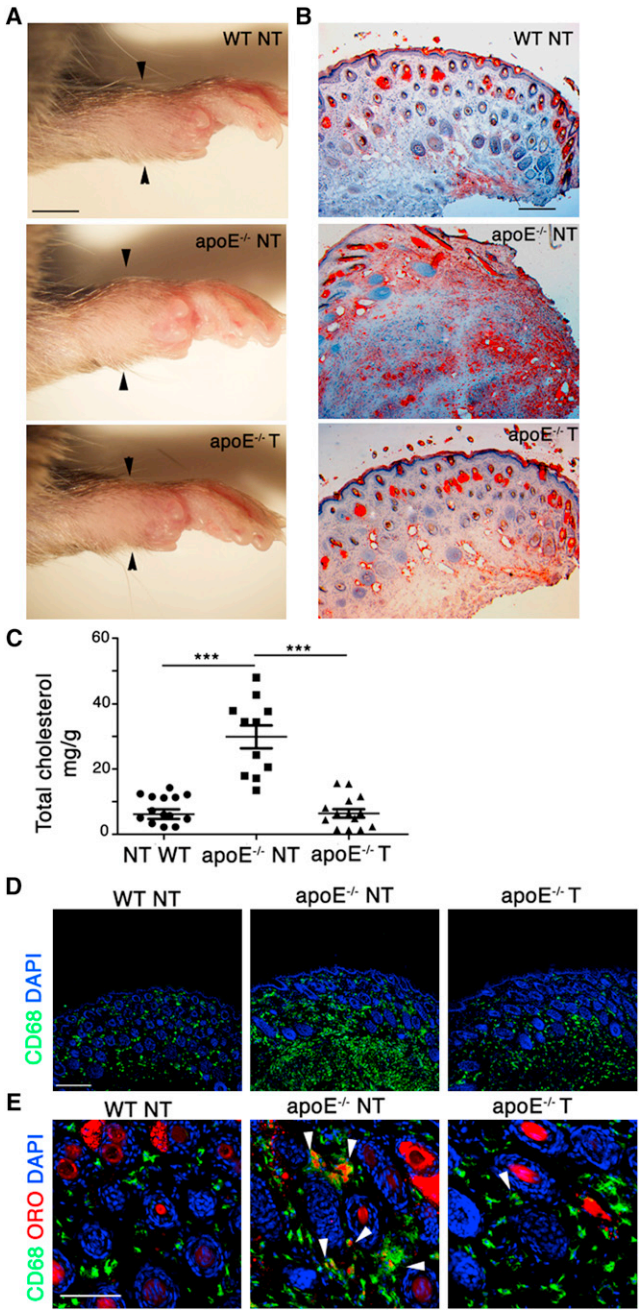

Figure 2. Diminution of Peripheral Lipid Accumulation in apoE$^{-/-}$ Mice with Improved Lymphatic Drainage

(A) Compared to those of WT and T apoE$^{-/-}$ mice, the footpads of NT-apoE$^{-/-}$ mice were edematous (arrowheads). The scale bar represents 2 mm.

(B) Oil red O staining of footpad skin sections demonstrated that edema in NT apoE$^{-/-}$ mice was associated with increased lipid accumulation. The scale bar represents 200 μm.

(A and B) Images are representative of two repeated experiments, and n = 4 per group.

(C) Total cholesterol levels were analyzed in footpads from NT WT and apoE$^{-/-}$ mice and T apoE$^{-/-}$ mice. Data are expressed as mean ± SEM with n = 11–16 per group. ***p < 0.0005.

(D and E) Footpad skin sections from WT, NT, and T apoE$^{-/-}$ mice were stained for CD68 (D). Costaining of CD68 with oil red O showed more macrophages loaded with lipids (arrowheads) in NT apoE$^{-/-}$ mice compared to NT WT and T-apoE$^{-/-}$ mice (E). Similar findings were observed in two independent experiments, and n = 2 per group. Scale bars represent 200 μm. See also Figure S2.

fluorescent cholesterol was primarily in HDL fraction (Figure S3D). Finally, we evaluated RCT in WT mice in which lymphatic drainage was altered by cutting of afferent lymphatic vessels draining from the footpad to the popliteal LN (Figure S3E). Notably, the clearance of cholesterol from the site of cholesterol-loaded macrophage deposition and its transport to lymph, blood, liver, and feces was markedly impaired in mice with excised lymphatic vessels (Figures 4G–4K). Impairing lymphatic drainage in WT mice impaired not only RCT of fluorescent cholesterol but also the transport of tissue cholesterol (Figure 4L). However, this effect was not accompanied by changes in plasma cholesterol (Figure 4L). Because apoE$^{-/-}$ mice exhibit impaired lymphatic transport, we tested whether RCT of fluorescent cholesterol may be affected in these mice. The transport of fluorescent cholesterol from the site of its deposition to plasma and liver was markedly compromised in apoE$^{-/-}$ mice (Figures 4M–4R). However, ameliorating lymphatic function in apoE$^{-/-}$ by either ezetimibe (Figures 4M–4O) or VEGF-C (Figures 4P–4R) treatment significantly improved RCT of fluorescent cholesterol.

Because HDL acts as an extracellular acceptor of cholesterol and mediates the transport of excess cholesterol from peripheral tissues to the liver, we verified that lymphatic vessels could transport HDL. Consistent with reports in human lymph (Cooke et al., 2004; Nanjee et al., 2001), we were able to detect the presence of HDL in lymph canulated from the cisterna chyli of 8-week-old WT mice. HDL concentration in lymph (29.48 ± 6.50 mg/dl, n = 5) was similar to HDL concentration in plasma (35.95 ± 1.52 mg/dl, n = 5). Next, we examined the transport of DiI-labeled HDL after subcutaneous injection into the rear footpad of WT mice. FITC-labeled dextran was coinjected with DiI-HDL to visualize lymphatic vessels (Figure 5A). Fluorescent images revealed that DiI-HDL colocalized with FITC-dextran and drained from the footpad to the popliteal LN via afferent lymph then into the next proximal iliac LN via efferent lymph and finally into the thoracic duct which drains to the blood circulation (Figure 5A). More importantly, the clearance of HDL from the footpad was significantly impaired (Figure 5B), and its subsequent accumulation in the draining LN and plasma was reduced by 90% and 80%, respectively, in mice with surgically impaired lymphatic drainage compared to sham-operated animals (Figures 5C and 5D). Improvement of lymphatic drainage in apoE$^{-/-}$ mice by ezetimibe or VEGF-C treatment significantly ameliorated the transport of DiI-HDL (Figure 5E and 5F).

Lymphatic Endothelial Cells Express Functional HDL Transporters

The finding that HDL can be transported in vivo by lymphatic vessels raised the possibility that the entry of cholesterol into lymphatics may be mediated by HDL-associated transporters (Tall, 2008) including SR-BI, ABCA1, and ABCG1. Quantitative real-time PCR analysis of the expression of these transporters on the murine lymphatic endothelial cell line, SV-LECs, (Ando et al., 2005) revealed that SR-BI and ABCA1, but not ABCG1, were expressed in SV-LECs (Figure 6A). The expression levels

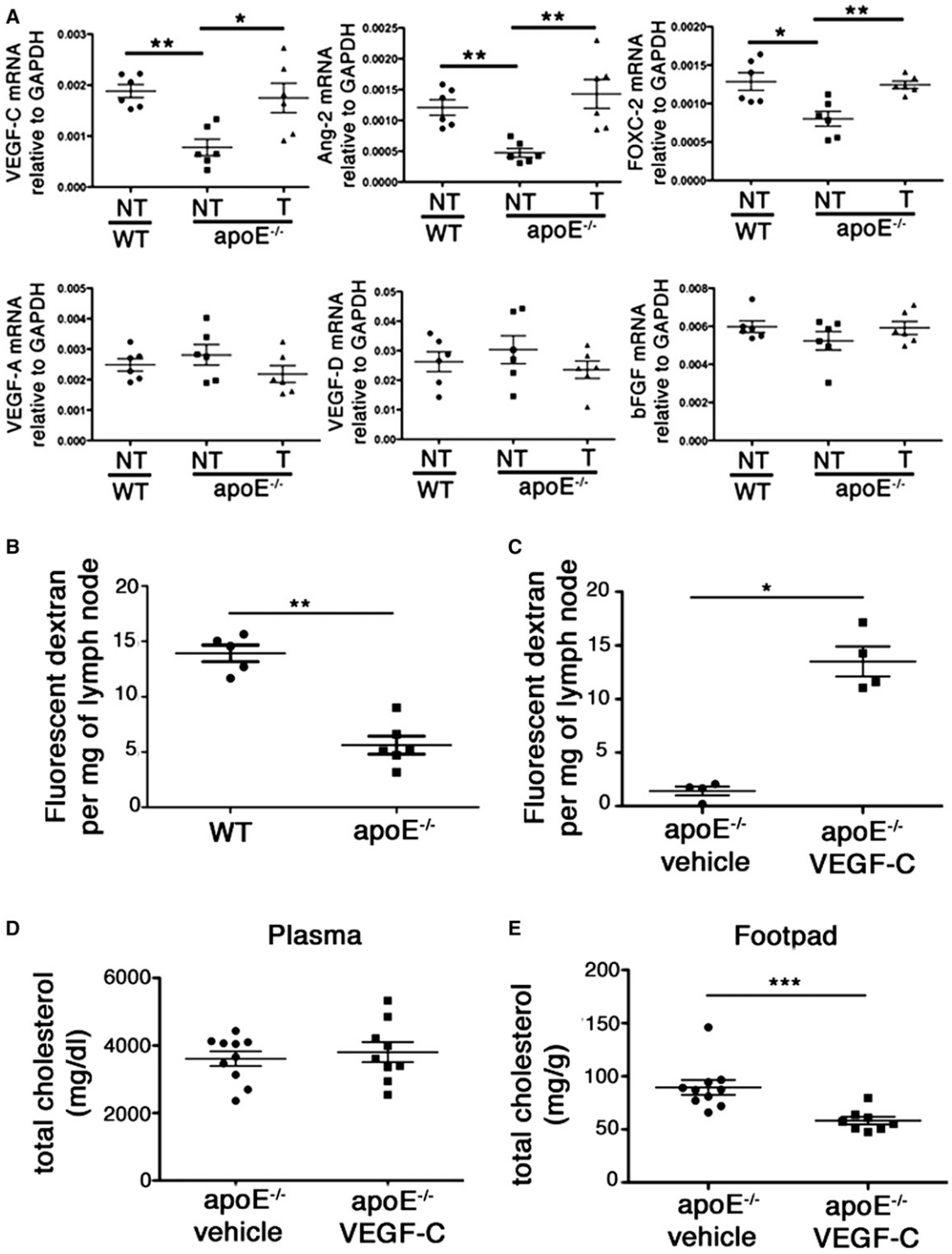

Figure 3. Improved Lymphatic Transport and Attenuated Peripheral Lipid Accumulation in apoE$^{-/-}$ Mice Treated with VEGF-C

Total mRNA extracted from the ear skin of vehicle (NT)- or ezetimibe (T)-treated WT and apoE$^{-/-}$ mice were evaluated by quantitative real-time PCR (A). Results collected from two independent experiments (n = 6). WT and apoE$^{-/-}$ (B) or vehicle- and VEGF-C-treated apoE$^{-/-}$ (C) FITC-dextran content in draining LNs was evaluated 10 min after injection in footpad. Total cholesterol levels were measured in the plasma (D) and footpads (E) from vehicle- and VEGF-C-treated apoE$^{-/-}$ mice. Data expressed as mean ± SEM with n = 4–10 per group. *$p < 0.05$, **$p < 0.005$, and ***$p < 0.0005$.

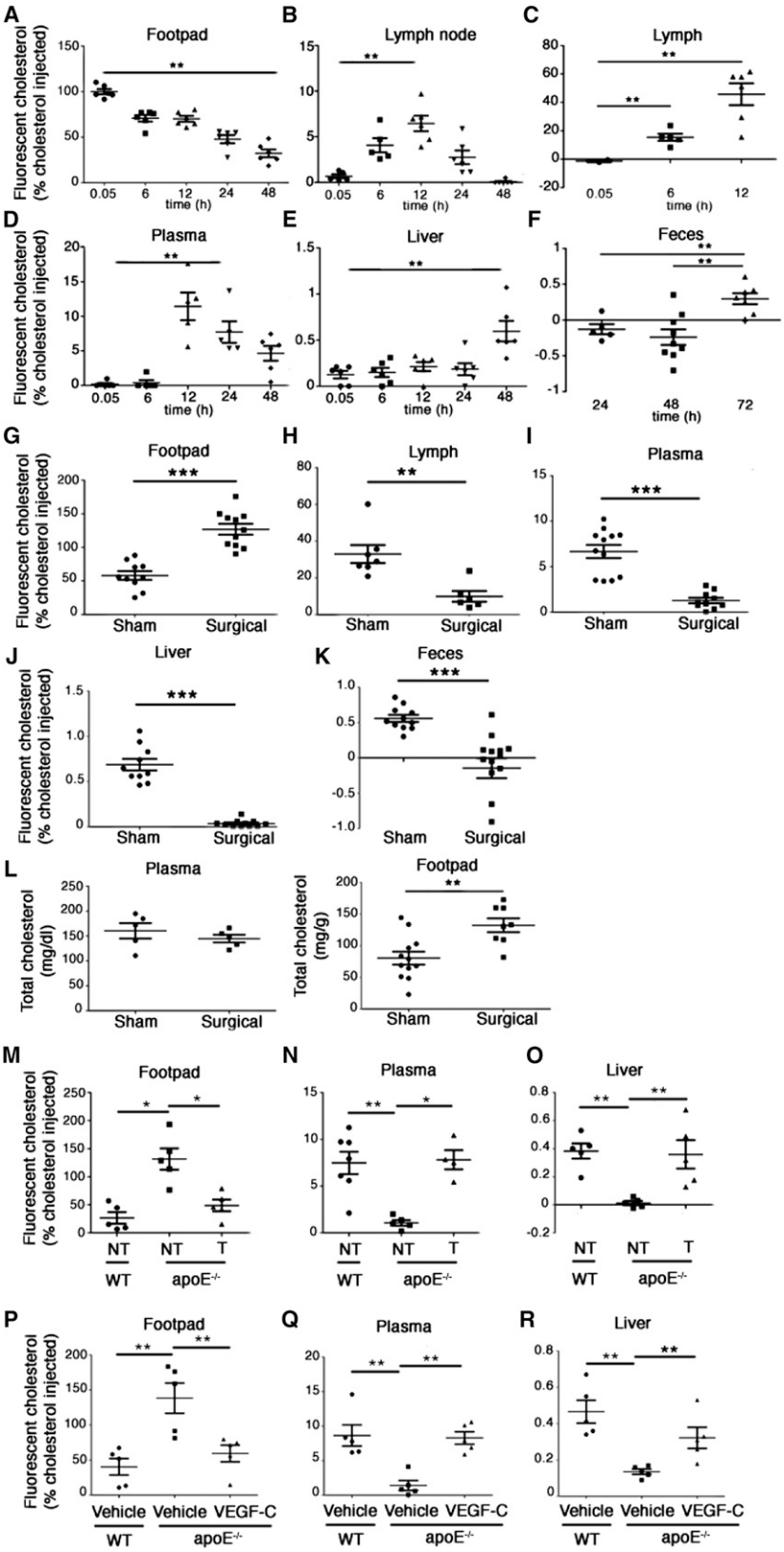

Figure 4. Inhibition of RCT in Mice with Impaired Lymphatic Drainage

(A–K) WT mice received footpad injections of fluorescent-cholesterol-loaded macrophages. Content in fluorescent cholesterol was evaluated 5 min and 6, 12, 24, and 48 hr after injection in footpad (A), LN (B), lymph (C), plasma (D), and liver (E). Feces were collected continuously from 0–24, 24–48, and 48–72 hr for fluorescent-cholesterol measurements (F). Twenty-one days after surgery (see Figure S3E), sham and surgical-operated animals received fluorescent-cholesterol-loaded macrophages. Fluorescent cholesterol was evaluated at 48, 12, 24, 48, and 48–72 hr in footpad (G), lymph (H), plasma (I), liver (J), and feces (K), respectively. Data are expressed as the percentage of fluorescent cholesterol relative to total fluorescent cholesterol detected at 5 min in the footpad (site of injection).

(L) Total cholesterol content in the plasma and footpad from sham and surgical-operated mice were analyzed. (M–R) RCT was assessed in apoE$^{-/-}$ mice treated with vehicle, ezetimibe (M–O) or VEGF-C (P–R) as described in Figures 1 and 3 by measurement of fluorescent cholesterol in footpad (M and P), plasma (N and Q), and liver (O and R).

Data were collected from two to six independent experiments with n = 5–12 per group and are shown as mean ± SEM; *p < 0.05, **p < 0.005, ***p < 0.0005. See also Figure S3.

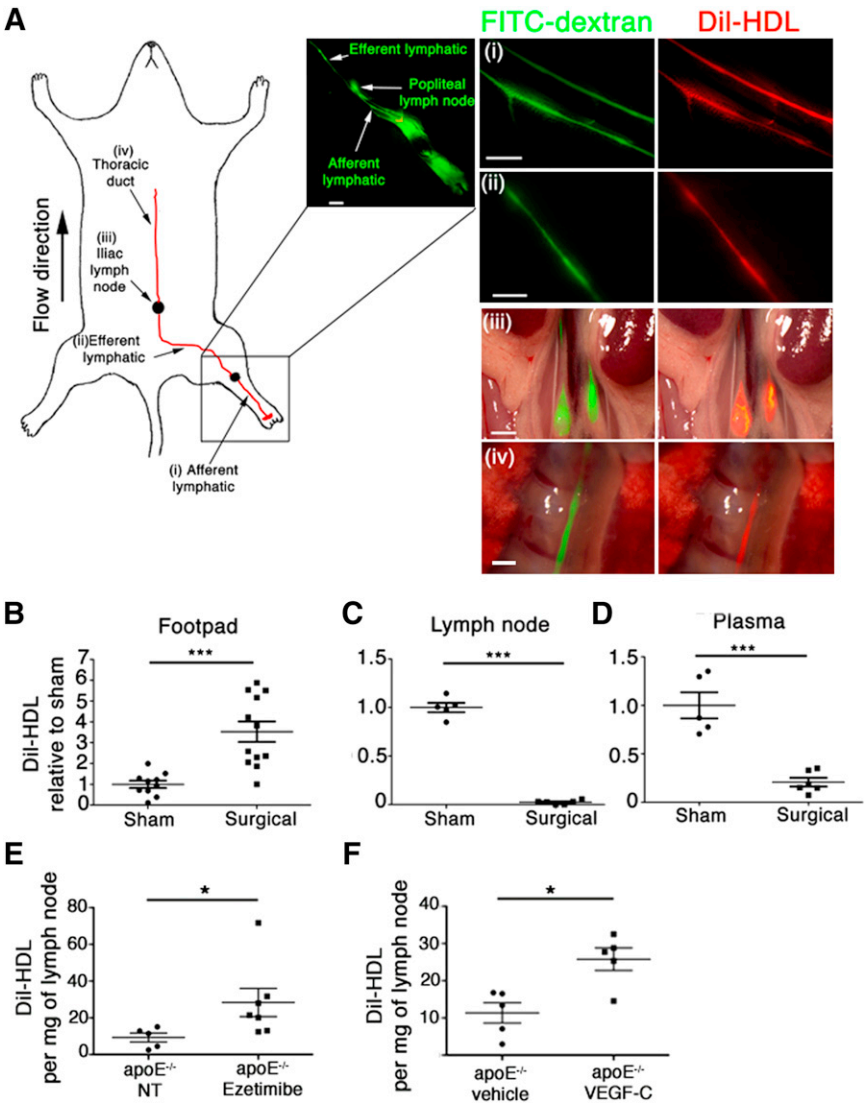

Figure 5. Impaired Transport of HDL from Peripheral Tissues by Obstruction of Lymphatic Drainage

(A) Transport of Dil-HDL from footpad to thoracic duct via lymphatic vessels was assessed. For visualization of lymphatic vessels, FITC-dextran was also coadministrated with Dil-HDL. Dil-HDL was transported from the footpad to the popliteal LNs via afferent (i) then efferent (ii) lymphatic vessel, into the next proximal iliac LNs (iii), and, subsequently, into the thoracic duct (iv). The same findings were observed in three repeated experiments. Scale bars represent 500 μm.

(B–D) Lymphatic vessel flow was disrupted in WT mice, and 12 days after, Dil-HDL was subcutaneously injected in the footpad. One hour later, footpads (B), LNs (C), and plasma (D) were collected for measurement of Dil-HDL. Data are expressed as Dil-HDL relative to sham-operated groups and as mean ± SEM and pooled from two independent experiments with n = 6–12 per group. ***$p < 0.0005$.

(E and F) Quantification of Dil-HDL transport to LNs was performed on NT and T ezetimibe apoE$^{-/-}$ (E) or vehicle- and VEGF-C treated apoE$^{-/-}$ (F) mice. Data were collected from two independent experiments with n = 5–7. *$p < 0.05$. Data are shown as mean ± SEM.

of SR-BI and ABCA1 in LECs were similar to RAW macrophage cell lines, which served as positive control (Lorenzi et al., 2008). Microscopic (Figure 6B) and flow-cytometric (Figure 6C) immunofluorescence analyses for SR-BI and ABCA1 confirmed that SV-LECs expressed these two HDL transporters at their surface. Confocal fluorescence microscopy of SV-LECs revealed that HDL was internalized by LECs as soon as 10 min after incubation with Dil-HDL, and this was even more apparent at 30 and 60 min (Figure 6D). Internalization of HDL in LECs was confirmed by the partial colocalization of vesicles containing Dil-HDL with Alexa 488 transferrin (Figure 6E).

Downregulation of SR-BI expression in SV-LECs but not ABCA1 by RNA interference significantly impaired HDL uptake, corresponding to 80% inhibition of HDL uptake (Figure 6F). To further confirm these results, we measured the effect of a blocking antibody against SR-BI or a specific chemical inhibitor, BLT1, on HDL uptake. Incubation with SR-BI antibody inhibited Dil-HDL uptake by SV-LECs analyzed 10 and 60 min after the incubation with Dil-HDL (Figure 6G). A similar effect on HDL internalization by SV-LECs was observed after incubation with BLT1 (Figure S4A).

Next, we studied whether HDL can be transported through a monolayer of LECs. For this assay, the lipid and apolipoprotein components of HDL were labeled with Dil and Alexa 488, respectively, and this dual-labeled HDL was added on the top of the SV-LEC monolayer. A significant amount of Dil-HDL and Alexa-488-HDL was transported 1 hr after incubation with dual labeled HDL into the bottom compartment at 37°C (Figure 6H). In contrast, the transport of Dil-HDL and Alexa-488-HDL was markedly diminished at 4°C, a temperature known to prevent internalization (Rohrer et al., 2009), suggesting HDL is transcytosed through LECs (Figure 6H). Pretreatment of SV-LECs with anti-SR-BI blocking antibody significantly inhibited the transport of dual labeled HDL through LEC monolayer (Figure 6I) but did not affect the transport of FITC-dextran (Figure 6J). Expression of SR-BI, internalization of HDL, and involvement of SR-BI in mediating HDL transport through a monolayer of LECs were also observed in human primary dermal LECs, supporting the relevance of our findings in human physiology (Figures S4B–S4E).

HDL Transport by Lymphatic Vessels Involves SR-BI

Here, we evaluated in vivo the relevance of our in vitro findings. Consistent with our observations in SV-LECs, fluorescent microscopic and flow-cytometric analyses revealed the expression of SR-BI on podoplanin^{+} lymphatic vessels from skin of WT mice (Figures 7A and 7B). Then, we went on to test in vivo the effect

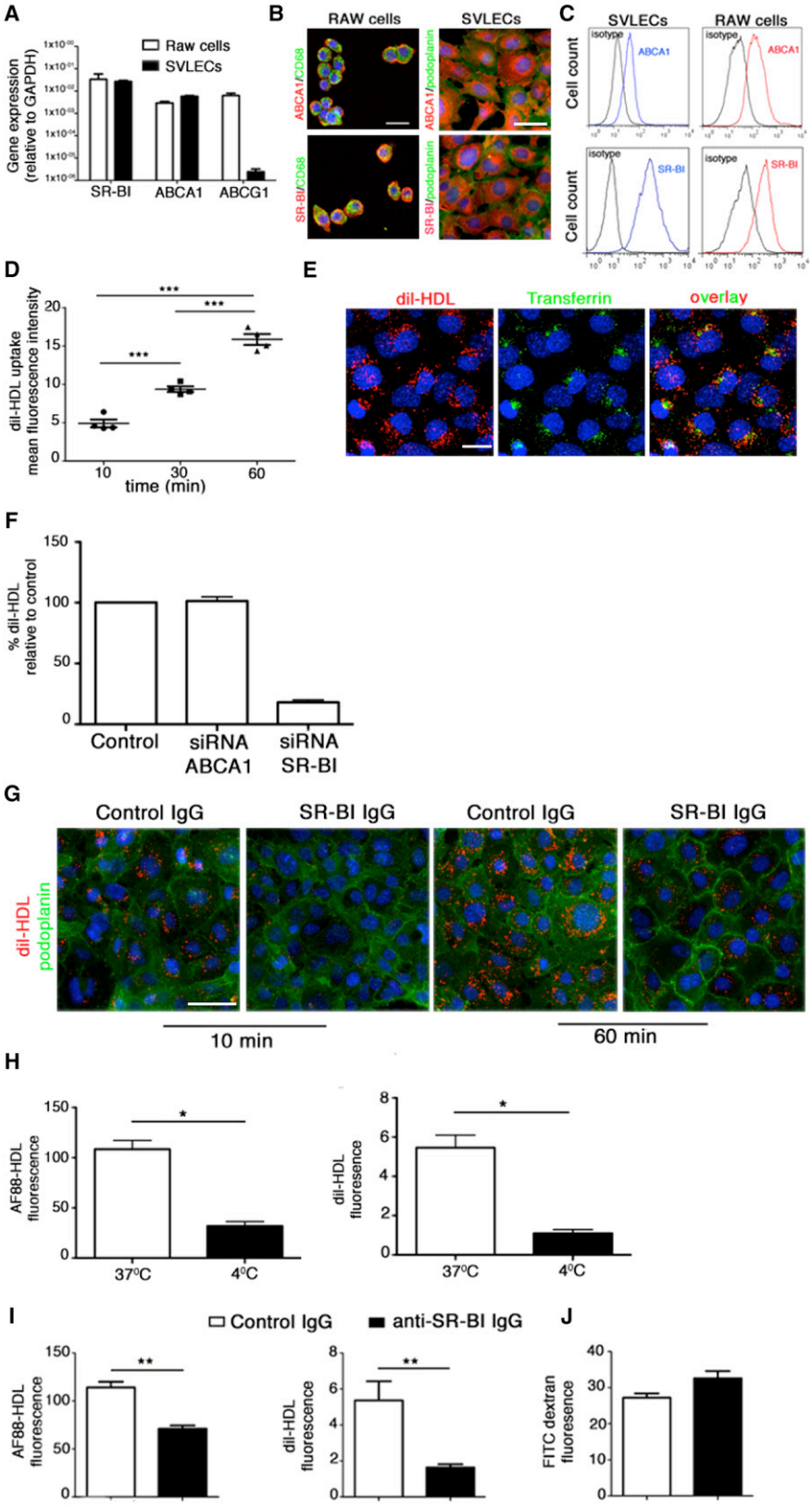

(legend on next page)

of SR-BI blocking antibody on the transport of HDL and RCT. Notably, we found that treatment of WT mice with SR-BI blocking antibody significantly inhibited the transport of HDL via lymphatic vessels since the accumulation of fluorescent signal in LN from SR-BI treated mice was reduced by 75% compared to untreated animals (Figure 7C). However, blocking SR-BI did not affect the transport of the macromolecule TRITC-dextran to the LN (Figure 7C). Finally, we demonstrated that RCT of fluorescent cholesterol in WT mice treated with SR-BI blocking antibody was significantly compromised (Figure 7D). That the levels of fluorescent cholesterol increased at 24 hr and 48 hr in plasma of SR-BI-antibody-treated mice compared to untreated mice is consistent with RCT studies in SR-BI-deficient mice reporting that cholesterol accumulates in the plasma as a result of blocking SR-BI mediated transport of cholesterol into the liver (Zhang et al., 2003). To further confirm these findings, we used mice with a targeted null mutation in *SR-BI* gene. As previously reported (Rigotti et al., 1997), total cholesterol and HDL levels were elevated in the plasma of 6- to 8-week-old heterozygous (SR-BI$^{+/-}$) or homozygous (SR-BI$^{-/-}$) mutants compared to age-matched WT mice (Figures S5A and S5B). Notably, RCT of fluorescent cholesterol was significantly inhibited in SR-BI$^{-/-}$ mice and in a lesser extend in SR-BI$^{+/-}$ mice (Figure 7E). Consistent with a previous report (Zhang et al., 2003) and our RCT results in mice treated with SR-BI-neutralizing antibody, fluorescent cholesterol accumulated in plasma at 24 hr and 48 hr in SR-BI$^{-/-}$ mice. Moreover, SR-BI$^{-/-}$ mice showed an accumulation of total cholesterol in skin (Figure 7F). The transport of HDL to LN by lymphatic vessels was also significantly impaired in SR-BI$^{+/-}$ and SR-BI$^{-/-}$ mice (Figure 7G). However, the deficiency in SR-BI did not alter the transport of TRITC dextran from the footpad to the draining LN (Figure 7H). Altogether, our findings demonstrate for the first time that lymphatic vessel can transport HDL cholesterol through a mechanism that is, at least in part, dependent on SR-BI.

DISCUSSION

RCT is necessary to maintain cellular homeostasis and protects against atherosclerosis (Rader et al., 2009). RCT is initiated when tissue macrophages efflux cholesterol to extracellular HDLs. This step is tightly regulated through the action of ABCA1, ABCG1, and SR-BI (Tall, 2008). After cholesterol efflux, HDL cholesterol is transported from the peripheral tissue back into the blood circulation and then taken up by the liver either directly via SR-BI or indirectly via low density lipoprotein receptors. In the final step of RCT, the majority of HDL-derived cholesterol is removed from the liver by secretion into the bile, after which it is excreted via the feces (Rader et al., 2009; Tall, 2008). The routes whereby HDL cholesterol travels from the peripheral tissues back to the circulation are still not well characterized. It has been suggested previously that RCT is so important biologically that it may utilize all available routes (Reichl and Miller, 1989). Here, we provide direct evidence that the return of cholesterol to the plasma can occur via the lymphatic system. We took advantage of the existence of fluorescence-labeled cholesterol (Lamant et al., 2006; Sparrow et al., 1999) and HDL to image in vivo their transport after they have been introduced into the subcutaneous tissue of healthy animals. This analysis revealed that both cholesterol and HDL travel from the skin back to the blood circulation via lymphatic vessels, draining LNs and the thoracic duct. Impairment of peripheral lymphatic drainage by surgical excision of afferent lymphatic vessels in WT mice potently abrogated the transport of fluorescence-labeled HDL to both draining LNs and plasma, trapping HDL in the peripheral site of injection. Furthermore, compromise of lymphatic function in our modified in vivo RCT model also markedly reduced the return of cholesterol to plasma and liver after cholesterol efflux from macrophages deposited in subcutaneous tissue. This is, to our knowledge, the first report to show the pivotal contribution of lymphatic drainage in the initial step of RCT. In contrast, the venous capillary system does not seem sufficient to support the transport of HDL cholesterol back to the circulation, as previously anticipated (Reichl, 1990, 1994).

Next, we went on to investigate the mechanisms by which lymphatic vessels transport cholesterol, as they remain poorly studied despite the recent advances in our knowledge of lymphatic biology. With the exception of immune cell entry, it is generally thought that the lymphatic system maintains interstitial fluid homeostasis by allowing passive entry of macromolecules and fluid through blind-ended openings within the initial lymphatic vessels (Schulte-Merker et al., 2011). This study, unexpectedly, challenges this current view by demonstrating that cholesterol entry into the lymphatic vessels can be a controlled

Figure 6. In Vitro HDL Uptake by Lymphatic Endothelial Cells

(A) Gene expression of ABCA1, ABCG1, and SR-BI was analyzed in SV-LECs and RAW macrophages by quantitative real-time PCR. Data pooled from three independent experiments are expressed as gene expression relative to GAPDH.

(B) CD68^{+} RAW macrophages and SV-LECs (as identified by lymphatic marker podoplanin) costained for SR-BI and ABCA1. Similar findings were observed in 3 experiments. Scale bars represent 20 and 50 μm.

(C) Surface expression of SR-BI and ABCA1 was analyzed by flow cytometry on RAW cells and SV-LECs.

(D) DiI-HDL uptake by SV-LECs was quantified 10 min, 30 min, and 1 hr after incubation of DiI-HDL. ***$p < 0.0005$.

(E) SV-LECs were incubated with DiI-HDL for 1 hr followed by Alexa 488 transferrin for 30 min. The experiment was repeated two times with the same observation. The scale bar represents 20 μm.

(F) SV-LECs were transfected with either small interfering RNA against SR-BI or ABCA1 or negative control for 7 hr before incubation with DiI-HDL. Data are expressed as a percentage of fluorescence intensity relative to negative control and were pooled from three independent experiments.

(G) SV-LECs were preincubated with blocking SR-BI antibody or control IgG for 1 hr followed by incubation with DiI-HDL. SR-BI antibody but not control IgG inhibited DiI-HDL uptake by SV-LECs. Images are representative of five repeated experiments (n = 3 per group). The scale bar represents 50μm.

(H–J) HDL labeled with DiI and Alexa 488 (H and I) or FITC-dextran (J) was added on the top of SV-LECs cultured on inserts at 4°C and 37°C (H) or on top of SV-LEC inserts pretreated with SR-BI blocking antibody or control IgG at 37°C (I and J). After 1 hr, the supernatant from the bottom compartment was collected for fluorescence measurements. Data were pooled from three to seven inserts, and the experiments were repeated at least two times. *$p < 0.05$, **$p < 0.005$. Data are shown as mean ± SEM.

See also Figure S4 and Table S1.

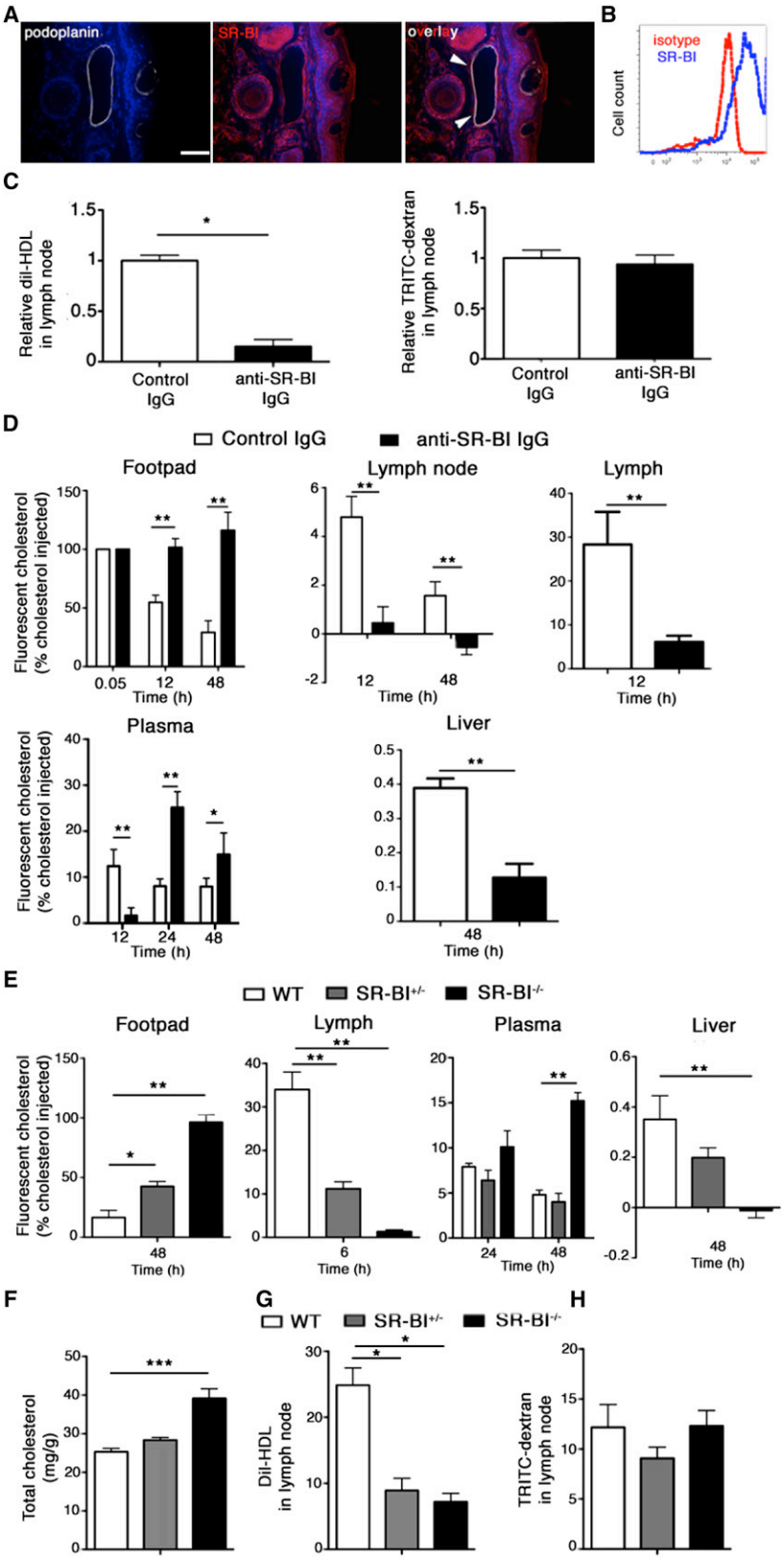

Figure 7. SR-BI-Mediated Reverse Cholesterol Transport by Lymphatic Vessels

(A) Skin sections from WT mice were stained for SR-BI and podoplanin. Arrows indicate a lymphatic vessel. A similar finding was observed in four repeated experiments. The scale bar represents 50 μm.

(B) Cell suspension from mouse ear dermis was stained for CD45, podoplanin, CD31, and SR-BI to assess the expression of SR-BI on LECs ($CD45^{-}CD31^{+}$ $podoplanin^{+}$).

(C) WT mice were treated with either SR-BI blocking antibody or control IgG, and 12 hr later, either Dil-HDL or TRITC-dextran was injected into the rear footpads. Draining LNs were collected 1 hr and 10 min later for Dil-HDL and TRITC-dextran, respectively, for evaluation of the fluorescent tracer. Data are expressed as relative fluorescent tracer to control IgG and were compiled from two independent experiments with n = 5–6 per group. *$p < 0.05$.

(D and E) Control IgG and SR-BI blocking antibody treated WT mice (D) or $SR\text{-}BI^{+/-}$ and $SR\text{-}BI^{-/-}$ mice (E) received footpad injection of fluorescent-cholesterol-loaded macrophages, and the fluorescent-cholesterol content was evaluated in footpad, LN, lymph, plasma, and liver. Data are expressed as the percentage of fluorescent cholesterol relative to total fluorescent cholesterol detected at 5 min in the footpad (site of injection) and were collected from two independent experiments with n = 5–8 per group.*$p < 0.05$, **$p < 0.005$.

(F) Total cholesterol levels were analyzed in footpads from WT, $SR\text{-}BI^{+/-}$ and $SR\text{-}BI^{-/-}$ mice. n = 7–14 per group. ***$p < 0.0005$.

(G and H) WT, $SR\text{-}BI^{+/-}$, and $SR\text{-}BI^{-/-}$ mice received Dil-HDL (G) or TRITC-dextran (H) into the rear footpads, and draining LNs were collected 1 hr and 10 min later, respectively, for evaluation of the fluorescent tracer. Data were compiled from two independent experiments with n = 3–5 per group. *$p < 0.05$. Data are shown as mean ± SEM.

See also Figure S5.

and active process—namely, HDL entry through lymphatic vessels is mediated via SR-BI. This scavenger receptor is ubiquitously expressed in several organs, and its function in cholesterol metabolism is determined by the cell type. In the blood vessels, endothelial SR-BI has been shown to actively transport HDL from the vessel lumen into the peripheral tissues (Rohrer et al., 2009). In the intestines, SR-BI on enterocytes is involved in cholesterol uptake/binding, which could facilitate subsequent cholesterol absorption via NPC1L1 (Labonté et al., 2007). In the liver, hepatocyte SR-BI is important for the selective uptake of esterified and unesterified cholesterol carried by HDL (Zhang et al., 2005). Here, we demonstrate both in vitro and in vivo that SR-BI is expressed by lymphatic endothelium and mediates the internalization and transport of HDL. Although passive entry into the lymphatic vessels may also contribute to HDL transport, inhibition or absence of SR-BI markedly reduced in vivo the transport of HDL from the interstitium to the draining LNs and RCT, demonstrating that entry of interstitial HDL through lymphatic vessels depends on SR-BI and probably outweighs passive entry. Furthermore, since the loss of SR-BI activity had no apparent effect on the transport of the macromolecule TRITC-dextran both in vivo and in vitro and was not compensated by the presence of ABCA1 expressed by lymphatic endothelial cells, these findings further support the specific function of SR-BI in lymphatic endothelium for the uptake of HDL. We next addressed whether the transport of cholesterol through lymphatics involves the intercellular pathway, currently considered to be the major pathway (Schmid-Schönbein, 1990) or the transendothelial pathway. This latter pathway, which has been recently proposed as an additional pathway for the entry of macromolecules in lymphatic vessels, may be mediated by vesicles, which are abundant in lymphatic endothelium (Leak, 1976; Podgrabinska et al., 2002). Supporting this possible mechanism, tracer particles injected in the interstitium of animals have been identified within the vesicles of initial lymphatic vessels (Feng et al., 2002; Leak, 1976). Our study on the transport of dual labeled HDL through a monolayer of LECs reveals that the transport of both the protein and lipid component of HDL involves, at least in part, the transendothelial pathway and SR-BI, suggesting that unlike on hepatocytes, SR-BI on LECs does not selectively uptake cholesterol carried by HDL.

Here, we show that the structural alterations in lymphatic vessels of apoE$^{-/-}$ mice are associated with the decreased expression of FOXC2 and VEGF-C. Furthermore, improvement of lymphatic function in apoE$^{-/-}$ mice by reduction of hypercholesterolemia with ezetimibe markedly decreased cholesterol accumulation and edema in peripheral tissues of these mice. These data further support this two-way relationship between cholesterol homeostasis and lymphatic function that we proposed previously (Lim et al., 2009) and demonstrate the essential role of lymphatic drainage in controlling the clearance of cholesterol in peripheral tissues. The decrease in cholesterol accumulation observed in the skin of apoE$^{-/-}$ mice treated with ezetimibe may result from both a decreased influx of cholesterol in the tissue as ezetimibe reduces total plasma cholesterol and an increased clearance of interstitial cholesterol by lymphatic drainage. However, our experiment in which apoE$^{-/-}$ mice were treated locally with VEGF-C revealed that restoring lymphatic function independently of lowering cholesterolemia can be sufficient to reduce the accumulation of cholesterol in the skin of apoE$^{-/-}$ mice by supporting RCT. Taken together, these studies in apoE$^{-/-}$ mice have direct clinical relevance and potential therapeutic applications. Indeed, the accumulation of lipid in skin from apoE$^{-/-}$ mice as characterized by massive infiltration of lipid-laden macrophages corresponds to a clinical skin feature, namely xanthoma (Frankel and Capone, 1995; van Ree et al., 1995). Several clinicians proposed that poor lymphatic drainage may further contribute to the formation of xanthomas (Berger et al., 1972; Hunter et al., 1970; Polano, 1969). This association between poor lymphatic drainage and xanthomas was further strengthened by clinical studies reporting that the use of compression garments to resolve lymphedema ameliorate xanthomatous eruptions in these normolipidemic patients (Berger et al., 1972). Notably, about half of the patients with xanthomas have primary or secondary lipid disorders, and the presence of xanthomas often serves as an important basic criterion in the clinical diagnosis of primary dyslipidemia, such as familial hypercholesterolemia (Goldberg et al., 2011; Frankel and Capone, 1995). However, it remains unknown whether the interconnection between lymphatic dysfunction and xanthomas formation also holds in patients with dyslipidemia. Our data showing that restoration of lymphatic vessel function in dyslipidemic apoE$^{-/-}$ mice with ezetimibe decreased xanthomas supports this concept and provides strong evidence for the beneficial effect of improving lymphatic drainage in patients with xanthomas with or without dyslipidemia. Moreover, our data revealing that the structural and functional defects in lymphatics from apoE$^{-/-}$ mice were associated with decreased expression of FOXC2 are in strong agreement with a recent clinical study in patients with familial combined hyperlipidemia. Indeed, these dyslipidemic patients exhibited alterations in lymphatic vessels and lower gene expression of FOXC2 and Prox-1 in their adipose tissues (Horra et al., 2009).

In conclusion, we provide direct evidence for the implication of lymphatic vessels in the initial steps of RCT and that lymphatic transport of cholesterol is an active process involving SR-BI. These findings reveal lymphatic vessels as potential targets for lipid-related diseases, including atherosclerosis, diabetes, and familial hypercholesterolemia, and thus the need for increased research on lymphatic function and lipid metabolism.

EXPERIMENTAL PROCEDURES

Cells and Mice

SV-LECs provided by Dr. J.S. Alexander were cultured as previously described (Ando et al., 2005). Primary human dermal LEC and RAW264.7 macrophages were purchased from Lonza Australia (Mount Waverly, VIC, Australia) and ATCC, respectively. ApoE$^{-/-}$, Ldlr$^{-/-}$, and SR-BI$^{+/-}$ mice on a C57BL/6 background were obtained from Jackson Laboratory (Bar Harbor, ME), fed different diet and treated in some experiments with ezetimibe or VEGF-C as described in the Supplemental Experimental Procedures. All experiment procedures were approved by the institutional animal care and use committees of the National University of Singapore.

Lymphatic Functional Assessment

Lymphatic function was assessed using Evans blue dye for tracing cutaneous lymphatic vessels as described previously (Lim et al., 2009).

Dendritic Cell Migration Assay

Migration of dendritic cell to LN was evaluated after epicutaneous application of FITC solution as described previously (Angeli et al., 2004).

Immunohistochemistry

Whole-mount immunohistochemical analysis of the ear skin to visualize initial and collecting lymphatic vessels was performed as described previously (Lim et al., 2009). For analysis of the expression of SR-BI on mouse tail skin, specimens were fixed in 2% paraformaldehyde (PFA) and 30% sucrose overnight at 4°C and frozen in Tissue-Tek Optimum Cutting Temperature compound for 10 μm cryosectioning. Immunostaining was performed with a Tyramide signal amplification kit (Perkin Elmer) according to manufacturer's instruction and with rabbit anti-mouse SRB1 (rabbit polyclonal; Novus Biologicals) revealed with rabbit horseradish peroxidase followed by Cy3-conjuagted Tyramide. Costaining with Syrian hamster anti-mouse podoplanin (clone 8.1.1; Developmental Studies Hybridoma Bank) antibody followed by AF488-conjugated secondary antibodies (Jackson Immunoresearch) was used to identify lymphatic vessels. For SR-BI and ABCA1 staining on SV-LECs and RAW macrophages cultured on glass coverslips, cells were fixed in 4% PFA for 10 min followed by staining with Syrian hamster anti-podoplanin and rabbit anti-mouse SRB1 or ABCA1 polyclonal antibodies (Novus Biologicals). For lipid staining, cryosections of mouse footpad skin were stained with hematoxylin and oil red O. For identification of foam cells, skin sections were stained with macrophage marker CD68 (rat clone FA-11; Serotec) followed by oil red O staining, which was visualized as pseudocolored red under the Texas Red filter.

Specimens were viewed with a fluorescence wide field (Axio Imager.Z1, Axioxam HRM camera; Carl Zeiss Micro Imaging, Jena, Germany) or confocal microscope (Leica TCS SP5; Leica Microsystems, Deerfield, IL) with LAS AF confocal software (version 1.8.2; Leica Microsystems). Morphometric measurements of initial lymphatic vessel diameter were performed as previously described with Image J (Lim et al., 2009).

Disruption of Lymphatic Flow

A solution of 1% Evans Blue (Sigma) was injected into the hind-limb footpads for visualization of lymphatic vessels. In the "surgical-operated" animal group, at least a 2 mm length of afferent lymphatic vessels draining the popliteal LN was surgically cut (Ikomi et al., 2008), while lymphatic vessels in the "sham-operated" animal group were left exposed in the same way but not cut. Mice were used 12–21 days later for HDL uptake and RCT.

Reverse Cholesterol Transport

22-NDB-cholesterol, a fluorescent analog of cholesterol (Molecular Probes), was the preferred choice for our study because its uptake and efflux by/from macrophages closely resemble that of radiolabeled cholesterol (Lamant et al., 2006; Sparrow et al., 1999). We adapted the RCT protocol developed by the laboratory of Rader (Wang et al., 2007; Zhang et al., 2003). RAW264.7 macrophages were treated overnight with 5 μg/ml 22-NDB cholesterol, and cholesterol efflux was evaluated as described in the Supplemental Experimental Procedures. Mice received intraperitoneal or footpad subcutaneous injection of 0.5 ml or 20 μl, respectively, of 5×10^6 22-NDB-cholesterol loaded macrophages. The footpads, blood, lymph, LNs, and liver were collected 5 min and 12, 24, 48, and 72 hr later, whereas feces were collected continuously from 24–48 and 48–72 hr later. Samples were then processed as described in the Supplemental Experimental Procedures to measure cholesterol fluorescence. Data were expressed as fluorescence intensity per μg of tissue weight. Samples from mice receiving injection of noncholesterol loaded macrophages were used as blanks.

In Vitro and In Vivo SR-BI Blockade

SR-BI was block in vitro and in vivo with the chemical inhibitor BLT1 (Sigma-Aldrich) or a specific blocking antibody (Novus Biological, NB400-113) at doses known to be effective. The effect of blocking SR-BI on RCT, HDL, and FITC-dextran transport was evaluated as described in the Supplemental Experimental Procedures.

In Vivo and In Vitro Lymphatic Uptake of HDL

To assess HDL transport in vivo or its uptake by SV-LECs or human LECs in vitro, we used Dil-HDL (Biomedical Technologies) that was further labeled with Alexa 488 (Molecular Probes kit) for some experiments or reconstituted Alexa-488-labeled HDL (rHDL; containing 1-palmitoyl-2-linoleoylphosphatidylcholine and apolipoprotein A-I prepared by cholate dialysis) as described in the Supplemental Experimental Procedures.

HDL Transport through SV-LEC or Human LEC Monolayer

SV-LECs and human LECs were cultured on polyester membrane transwell cell culture inserts (0.4 μm, Corning, NY) coated with collagen type I (BD, North Ryde, NSW, Australia). In some experiments, cells were preincubated with anti-SRB1 antibody, diluted 1/100 in serum-free media for 1 hr. For experiments with SV-LECs, Dil-HDL was further labeled with an Alexa 488 protein labeling kit (Invitrogen), and 30 μg/ml on this dual-labeled HDL or FITC dextran was added on top of SV-LEC inserts for 1 hr at 37°C or 4°C. For experiments with human LECs, cells were incubated with rHDL consisting of Alexa-488-labeled apolipoproteinA-I (final concentration 10 μg/ml) for 10 min at 37°C. Then, 100 μl medium from the bottom well was removed for quantification of the fluorescence signal (excitation 490 nm, emission 520 nm).

Quantitative Real-Time PCR

Real-time PCR was performed with SYBR Green PCR Master Mix (Applied Biosystems) and analyzed on an Abi Prism 7500 Detection System (Applied Biosystems, Warrington, UK) or the CFX96 Real-Time PCR detection system (Bio-Rad) for mouse and human samples, respectively. The primers used are listed in Table S1.

Small Interfering RNA Transfection

For silencing of ABCA1 or SRB1, a mixture containing small interfering RNA for ABCA1 (100 nM), SRB1 (100 nM), or AllStars negative control (50 nM or 100 nM; QIAGEN) and DMEM without serum and HiPerfect (QIAGEN) was prepared for the transfection performed according to the manufacturer's protocol (QIAGEN). Transfection efficiency of SV-LECs was analyzed as described in the Supplemental Experimental Procedures.

Flow-Cytometric Analysis of SR-BI and ABCA1 Expression

SV-LECs and RAW cells and primary lymphatic endothelial cells from mouse ear skin isolated as described in the Supplemental Experimental Procedures, were stained with rabbit anti-mouse ABCA1 or SR-BI followed by anti-rabbit APC. FACS analysis was performed with a CyAn ADP Analyzer (Beckman Coulter) and data were analyzed with Flowjo software (Treestar).

Statistical Analysis

Statistical Analysis was performed with Graphpad Prism version 5.0 (GraphPad Software). All the data were presented as mean ± SEM and were statistically analyzed by nonparametric Mann-Whitney U test. A p value of less than 0.05 was considered to be statistically significant.

SUPPLEMENTAL INFORMATION

Supplemental Information includes five figures, one table, and Supplemental Experimental Procedures and can be found with this article online at http://dx.doi.org/10.1016/j.cmet.2013.04.002.

ACKNOWLEDGMENTS

We thank Prof. M. Krieger (MIT, Cambridge, MA) for providing SR-BI deficient mice, K.W.J. Ng for technical assistance, and J.S. Mohammed and Y.S. Soh for critical discussion. This work was supported by the BioMedical Research Council, National Medical Research Council, and National Research Foundation.

Received: April 20, 2012
Revised: November 6, 2012
Accepted: April 1, 2013
Published: May 7, 2013

REFERENCES

Ando, T., Jordan, P., Joh, T., Wang, Y., Jennings, M.H., Houghton, J., and Alexander, J.S. (2005). Isolation and characterization of a novel mouse lymphatic endothelial cell line: SV-LEC. Lymphat. Res. Biol. *3*, 105–115.

Angeli, V., Llodrá, J., Rong, J.X., Satoh, K., Ishii, S., Shimizu, T., Fisher, E.A., and Randolph, G.J. (2004). Dyslipidemia associated with atherosclerotic disease systemically alters dendritic cell mobilization. Immunity *21*, 561–574.

Armstrong, M.L., Mathur, S.N., Sando, G.N., and Megan, M.B. (1986). Lipid metabolism in xanthomatous skin of hypercholesterolemic rabbits. Am. J. Pathol. *125*, 339–348.

Baluk, P., Fuxe, J., Hashizume, H., Romano, T., Lashnits, E., Butz, S., Vestweber, D., Corada, M., Molendini, C., Dejana, E., and McDonald, D.M. (2007). Functionally specialized junctions between endothelial cells of lymphatic vessels. J. Exp. Med. *204*, 2349–2362.

Berger, B.W., Kantor, I., and Maier, H.S. (1972). Xanthomatosis and lymphedema. Arch. Dermatol. *105*, 730–731, passim.

Breslin, J.W., Gaudreault, N., Watson, K.D., Reynoso, R., Yuan, S.Y., and Wu, M.H. (2007). Vascular endothelial growth factor-C stimulates the lymphatic pump by a VEGF receptor-3-dependent mechanism. Am. J. Physiol. Heart Circ. Physiol. *293*, H709–H718.

Cooke, C.J., Nanjee, M.N., Stepanova, I.P., Olszewski, W.L., and Miller, N.E. (2004). Variations in lipid and apolipoprotein concentrations in human leg lymph: effects of posture and physical exercise. Atherosclerosis *173*, 39–45.

Danussi, C., Spessotto, P., Petrucco, A., Wassermann, B., Sabatelli, P., Montesi, M., Doliana, R., Bressan, G.M., and Colombatti, A. (2008). Emilin1 deficiency causes structural and functional defects of lymphatic vasculature. Mol. Cell. Biol. *28*, 4026–4039.

Davis, H.R., Jr., Compton, D.S., Hoos, L., and Tetzloff, G. (2001). Ezetimibe, a potent cholesterol absorption inhibitor, inhibits the development of atherosclerosis in ApoE knockout mice. Arterioscler. Thromb. Vasc. Biol. *21*, 2032–2038.

Dixon, J.B. (2010). Lymphatic lipid transport: sewer or subway? Trends Endocrinol. Metab. *21*, 480–487.

Feng, D., Nagy, J.A., Dvorak, H.F., and Dvorak, A.M. (2002). Ultrastructural studies define soluble macromolecular, particulate, and cellular transendothelial cell pathways in venules, lymphatic vessels, and tumor-associated microvessels in man and animals. Microsc. Res. Tech. *57*, 289–326.

Frankel, R.M., and Capone, R. (1995). Xanthelasmas and xanthomas- cutaneous clues to systemic lipid disorders. Clin. Eye Vis. Care *7*, 117–128.

Goldberg, A.C., Hopkins, P.N., Toth, P.P., Ballantyne, C.M., Rader, D.J., Robinson, J.G., Daniels, S.R., Gidding, S.S., de Ferranti, S.D., Ito, M.K., et al. (2011). Familial hypercholesterolemia: screening, diagnosis and management of pediatric and adult patients: clinical guidance from the National Lipid Association Expert Panel on Familial Hypercholesterolemia. J. Clin. Lipidol. *5*, 133–140.

Horra, A., Salazar, J., Ferré, R., Vallvé, J.C., Guardiola, M., Rosales, R., Masana, L., and Ribalta, J. (2009). Prox-1 and FOXC2 gene expression in adipose tissue: A potential contributory role of the lymphatic system to familial combined hyperlipidaemia. Atherosclerosis *206*, 343–345.

Hunter, J.A., Morley, W.N., and Peterkin, G.A. (1970). Xanthomatosis secondary to lymphoedema. Trans. St Johns Hosp. Dermatol. Soc. *56*, 143–148.

Ikomi, F., Kawai, Y., Nakayama, J., Ogiwara, N., Sasaki, K., Mizuno, R., and Ohhashi, T. (2008). Critical roles of VEGF-C-VEGF receptor 3 in reconnection of the collecting lymph vessels in mice. Microcirculation *15*, 591–603.

Ishibashi, S., Goldstein, J.L., Brown, M.S., Herz, J., and Burns, D.K. (1994). Massive xanthomatosis and atherosclerosis in cholesterol-fed low density lipoprotein receptor-negative mice. J. Clin. Invest. *93*, 1885–1893.

Johnson, L.A., and Jackson, D.G. (2010). Inflammation-induced secretion of CCL21 in lymphatic endothelium is a key regulator of integrin-mediated dendritic cell transmigration. Int. Immunol. *22*, 839–849.

Kuhlencordt, P.J., Padmapriya, P., Rützel, S., Schödel, J., Hu, K., Schäfer, A., Huang, P.L., Ertl, G., and Bauersachs, J. (2009). Ezetimibe potently reduces vascular inflammation and arteriosclerosis in eNOS-deficient ApoE ko mice. Atherosclerosis *202*, 48–57.

Labonté, E.D., Howles, P.N., Granholm, N.A., Rojas, J.C., Davies, J.P., Ioannou, Y.A., and Hui, D.Y. (2007). Class B type I scavenger receptor is responsible for the high affinity cholesterol binding activity of intestinal brush border membrane vesicles. Biochim. Biophys. Acta *1771*, 1132–1139.

Lamant, M., Smih, F., Harmancey, R., Philip-Couderc, P., Pathak, A., Roncalli, J., Galinier, M., Collet, X., Massabuau, P., Senard, J.M., and Rouet, P. (2006). ApoO, a novel apolipoprotein, is an original glycoprotein up-regulated by diabetes in human heart. J. Biol. Chem. *281*, 36289–36302.

Leak, L.V. (1976). The structure of lymphatic capillaries in lymph formation. Fed. Proc. *35*, 1863–1871.

Lim, H.Y., Rutkowski, J.M., Helft, J., Reddy, S.T., Swartz, M.A., Randolph, G.J., and Angeli, V. (2009). Hypercholesterolemic mice exhibit lymphatic vessel dysfunction and degeneration. Am. J. Pathol. *175*, 1328–1337.

Lorenzi, I., von Eckardstein, A., Cavelier, C., Radosavljevic, S., and Rohrer, L. (2008). Apolipoprotein A-I but not high-density lipoproteins are internalised by RAW macrophages: roles of ATP-binding cassette transporter A1 and scavenger receptor BI. J. Mol. Med. *86*, 171–183.

Muthuchamy, M., and Zawieja, D. (2008). Molecular regulation of lymphatic contractility. Ann. N Y Acad. Sci. *1131*, 89–99.

Nanjee, M.N., Cooke, C.J., Wong, J.S., Hamilton, R.L., Olszewski, W.L., and Miller, N.E. (2001). Composition and ultrastructure of size subclasses of normal human peripheral lymph lipoproteins: quantification of cholesterol uptake by HDL in tissue fluids. J. Lipid Res. *42*, 639–648.

Petrova, T.V., Karpanen, T., Norrmén, C., Mellor, R., Tamakoshi, T., Finegold, D., Ferrell, R., Kerjaschki, D., Mortimer, P., Ylä-Herttuala, S., et al. (2004). Defective valves and abnormal mural cell recruitment underlie lymphatic vascular failure in lymphedema distichiasis. Nat. Med. *10*, 974–981.

Pflicke, H., and Sixt, M. (2009). Preformed portals facilitate dendritic cell entry into afferent lymphatic vessels. J. Exp. Med. *206*, 2925–2935.

Podgrabinska, S., Braun, P., Velasco, P., Kloos, B., Pepper, M.S., and Skobe, M. (2002). Molecular characterization of lymphatic endothelial cells. Proc. Natl. Acad. Sci. USA *99*, 16069–16074.

Polano, M.K. (1969). Cutaneous xanthomatosis in relation to the blood lipoprotein pattern. Br. J. Dermatol. *81*(*Suppl 2*), 2, 39–48.

Rader, D.J., Alexander, E.T., Weibel, G.L., Billheimer, J., and Rothblat, G.H. (2009). The role of reverse cholesterol transport in animals and humans and relationship to atherosclerosis. J. Lipid Res. Suppl. *50*, S189–S194.

Reichl, D. (1990). Lipoproteins of human peripheral lymph. Eur. Heart J. *11*(*Suppl E*), 230–236.

Reichl, D. (1994). Extravascular circulation of lipoproteins: their role in reverse transport of cholesterol. Atherosclerosis *105*, 117–129.

Reichl, D., and Miller, N.E. (1989). Pathophysiology of reverse cholesterol transport. Insights from inherited disorders of lipoprotein metabolism. Arteriosclerosis *9*, 785–797.

Reichl, D., Simons, L.A., Myant, N.B., Pflug, J.J., and Mills, G.L. (1973). The lipids and lipoproteins of human peripheral lymph, with observations on the transport of cholesterol from plasma and tissues into lymph. Clin. Sci. Mol. Med. *45*, 313–329.

Rigotti, A., Trigatti, B.L., Penman, M., Rayburn, H., Herz, J., and Krieger, M. (1997). A targeted mutation in the murine gene encoding the high density lipoprotein (HDL) receptor scavenger receptor class B type I reveals its key role in HDL metabolism. Proc. Natl. Acad. Sci. USA *94*, 12610–12615.

Roheim, P.S., Dory, L., Lefevre, M., and Sloop, C.H. (1990). Lipoproteins in interstitial fluid of dogs: implications for a role in reverse cholesterol transport. Eur. Heart J. *11*(*Suppl E*), 225–229.

Rohrer, L., Ohnsorg, P.M., Lehner, M., Landolt, F., Rinninger, F., and von Eckardstein, A. (2009). High-density lipoprotein transport through aortic endothelial cells involves scavenger receptor BI and ATP-binding cassette transporter G1. Circ. Res. *104*, 1142–1150.

Rutkowski, J.M., Moya, M., Johannes, J., Goldman, J., and Swartz, M.A. (2006). Secondary lymphedema in the mouse tail: Lymphatic hyperplasia, VEGF-C upregulation, and the protective role of MMP-9. Microvasc. Res. *72*, 161–171.

Schirger, A., Harrison, E.G., Jr., and Janes, J.M. (1962). Idiopathic lymphedema. Review of 131 cases. JAMA *182*, 14–22.

Schmid-Schönbein, G.W. (1990). Microlymphatics and lymph flow. Physiol. Rev. *70*, 987–1028.

Schulte-Merker, S., Sabine, A., and Petrova, T.V. (2011). Lymphatic vascular morphogenesis in development, physiology, and disease. J. Cell Biol. *193*, 607–618.

Schumann, K., Lämmermann, T., Bruckner, M., Legler, D.F., Polleux, J., Spatz, J.P., Schuler, G., Förster, R., Lutz, M.B., Sorokin, L., and Sixt, M. (2010). Immobilized chemokine fields and soluble chemokine gradients cooperatively shape migration patterns of dendritic cells. Immunity *32*, 703–713.

Sloop, C.H., Dory, L., and Roheim, P.S. (1987). Interstitial fluid lipoproteins. J. Lipid Res. *28*, 225–237.

Sparrow, C.P., Patel, S., Baffic, J., Chao, Y.S., Hernandez, M., Lam, M.H., Montenegro, J., Wright, S.D., and Detmers, P.A. (1999). A fluorescent cholesterol analog traces cholesterol absorption in hamsters and is esterified in vivo and in vitro. J. Lipid Res. *40*, 1747–1757.

Szuba, A., Skobe, M., Karkkainen, M.J., Shin, W.S., Beynet, D.P., Rockson, N.B., Dakhil, N., Spilman, S., Goris, M.L., Strauss, H.W., et al. (2002). Therapeutic lymphangiogenesis with human recombinant VEGF-C. FASEB J. *16*, 1985–1987.

Tal, O., Lim, H.Y., Gurevich, I., Milo, I., Shipony, Z., Ng, L.G., Angeli, V., and Shakhar, G. (2011). DC mobilization from the skin requires docking to immobilized CCL21 on lymphatic endothelium and intralymphatic crawling. J. Exp. Med. *208*, 2141–2153.

Tall, A.R. (2008). Cholesterol efflux pathways and other potential mechanisms involved in the athero-protective effect of high density lipoproteins. J. Intern. Med. *263*, 256–273.

Tammela, T., and Alitalo, K. (2010). Lymphangiogenesis: Molecular mechanisms and future promise. Cell *140*, 460–476.

van Ree, J.H., Gijbels, M.J., van den Broek, W.J., Hofker, M.H., and Havekes, L.M. (1995). Atypical xanthomatosis in apolipoprotein E-deficient mice after cholesterol feeding. Atherosclerosis *112*, 237–243.

Wang, X., Collins, H.L., Ranalletta, M., Fuki, I.V., Billheimer, J.T., Rothblat, G.H., Tall, A.R., and Rader, D.J. (2007). Macrophage ABCA1 and ABCG1, but not SR-BI, promote macrophage reverse cholesterol transport in vivo. J. Clin. Invest. *117*, 2216–2224.

Zhang, Y., Zanotti, I., Reilly, M.P., Glick, J.M., Rothblat, G.H., and Rader, D.J. (2003). Overexpression of apolipoprotein A-I promotes reverse transport of cholesterol from macrophages to feces in vivo. Circulation *108*, 661–663.

Zhang, Y., Da Silva, J.R., Reilly, M., Billheimer, J.T., Rothblat, G.H., and Rader, D.J. (2005). Hepatic expression of scavenger receptor class B type I (SR-BI) is a positive regulator of macrophage reverse cholesterol transport in vivo. J. Clin. Invest. *115*, 2870–2874.